High-Resolution Scanning Transmission Electron Tomography and Elemental Analysis of Zeptogram Quantities of Heterogeneous Catalyst

Paul A. Midgley,*,† John Meurig Thomas,*,†,‡ Lydia Laffont,† Matthew Weyland,† Robert Raja,§ Brian F. G. Johnson,§ and Tanya Khimyak§

Department of Materials Science and Metallurgy, University of Cambridge, Pembroke Street, Cambridge, CB2 3QZ U.K., Davy Faraday Research Laboratory, Royal Institution of Great Britain, 21 Albermarle Street, London, W1X 4BS U.K., and University Chemical Laboratory, University of Cambridge, Lensfield Road, Cambridge, CB2 1EW, U.K.

Received: January 17, 2004; In Final Form: February 26, 2004

The ability to visualize the three-dimensional structure of an object is of central importance in many branches of science and engineering. Recording an angular series of two-dimensional projections (images) and subsequently applying tomographic reconstruction methods has proven to be extremely successful at many lengthscales. Using scanning transmission electron microscopy (STEM) high angle annular dark field (HAADF) imaging, we describe how the three-dimensional distribution of bimetallic nanocatalysts (such as $Ru_{10}Pt_2$, diameter ~1 nm, mass 10^{-21} g) within mesoporous hosts may be precisely determined. Moreover, the simultaneous retrieval of the elemental composition (from electron-stimulated X-ray emission spectra) of individual catalytic nanoparticles was achieved.

Three-dimensional electron microscopy (3DEM) has been used in its various forms very successfully for over three decades to study the form and function of many biological structures.[1] One variant, electron tomography, where a series of images is acquired at successive tilts from a unique structure, has been used in the biophysical study of cells to shed light on their internal processes.[2,3] Conventionally, bright-field (BF) images are recorded in which the contrast has been enhanced using positive (or sometimes negative) staining or by heavily defocusing the image to introduce phase contrast. More recently, BF electron tomography has been applied to inorganic specimens particularly in the revelation of internal microcavities within zeolitic crystals.[4]

For a number of years some of us (J.M.T., B.F.G.J., R.R.)[5] have been developing new types of supported, bimetallic nanocatalyst that are exceptionally active in selective hydrogenation processes of key organic compounds, especially under solvent-free conditions.[5−7] Some of these catalysts, notably $Ru_{10}Pt_2$ (shown supported within a mesoporous silica structure in Figure 1), are capable of converting[8,9] biocatalytically generated intermediates (such as muconic acid) to adipic acid (a component of nylon and other synthetic fibers), demonstrating the feasibility of producing bulk chemicals from replenishable sources such as corn.[9,10] There is a pressing need to know more about the nature of these catalysts, in particular their composition, shape, location, and distribution within the filigree nanoporous silica,[6] the internal area of which is 800−1000 $m^2\ g^{-1}$.

For inorganic specimens, unlike (unstained) biological structures, for which high energy electron scattering can be described in the most part using a weak phase approximation, there is a large change in both the amplitude and phase of the scattered electron wave, which leads to strong diffraction contrast in a BF image. If the specimen is crystalline, then complications arising from bend contours or thickness fringes will be evident, but even in noncrystalline, three-dimensional specimens there will be considerable effects from Fresnel diffraction. Fresnel fringes seen at the specimen edge perturb the image contrast and will limit the attainable 3D resolution of the reconstruction. In general, for an inorganic specimen, a BF image does not strictly conform to the projection requirement required for electron tomography.[11]

By using scanning transmission electron microscopy (STEM) and recording high angle annular dark field (HAADF) images[12] with electrons scattered to high angles (Rutherford-type scat-

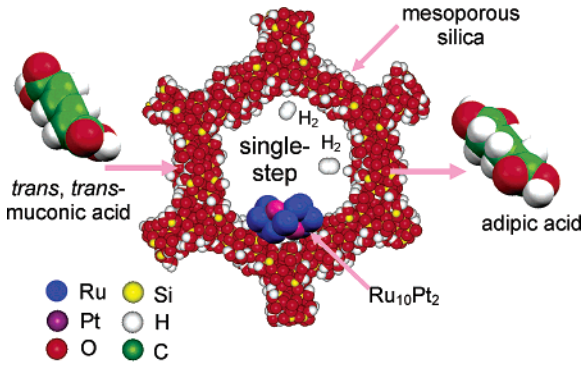

Figure 1. Schematic diagram illustrating the process of converting *trans*,*trans*-muconic acid, derived from glucose, to adipic acid, which is used in the manufacture of nylon. The catalyst is composed of bimetallic $Ru_{10}Pt_2$ nanoparticles anchored via two Pt−O and one Ru−O bonds (established[8] by X-ray absorption) to mesoporous silica (pore diameter 3 nm).

* Corresponding authors. P.A.M.: e-mail, pam33@cam.ac.uk; tel, +44 1223 334561; fax, +44 1223 334563. J.M.T.: jmt@ri.ac.uk.
† Department of Materials Science and Metallurgy, University of Cambridge.
‡ Royal Institution of Great Britain.
§ University Chemical Laboratory, University of Cambridge.

10.1021/jp049750b CCC: $27.50
Published on Web 03/19/2004

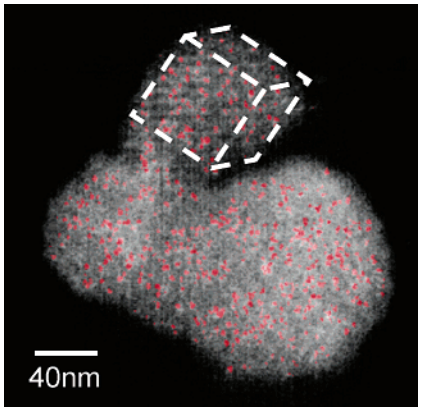

Figure 2. Perspective view (voxel projection) of a reconstruction of a heterogeneous catalyst composed of $Ru_{10}Pt_2$ active nanoparticles supported within a mesoporous silica framework.

tering) using an annular detector,[13] the problem of (Fresnel) diffraction contrast is minimized because of the loss of transverse coherence in electrons scattered to high angles.[13] In addition, the scattering cross-section is sensitive to the atomic number, Z (in the Rutherford limit this is Z^2), making it an ideal imaging mode for many heterogeneous systems. The two-dimensional resolution in a single HAADF image is given approximately by the probe size that can be subnanometer, and in aberration-corrected instruments even subangstrom, dimensions.[14] The development of combining STEM HAADF imaging with electron tomography[15,16] has introduced a powerful technique for 3D visualization at the nanometer scale.

A tilt series of HAADF STEM images was acquired[17] from a heterogeneous catalyst composed of bimetallic Pt−Ru particles[17] supported on and within a mesoporous silica framework. Figure 2 shows a voxel projection of a Pt/Ru−MCM41 catalyst in which the bimetallic particles are color-coded red and the mesoporous silica white. The porous nature (pore diameter ∼3 nm) has been well resolved and in this case it is clear that the structure has a high density of nanoparticles within the silica. An animation of the reconstruction is particularly revealing[17] (see Supporting Information online, movie S1). Parts a and b of Figure 3 show perpendicular views (voxel projections) at high-symmetry orientations of the cubic subvolume dotted in Figure 2. The hexagonal ordering of the silica mesopores is evident and emphasized in the power spectrum of the image; see inset of Figure 3a). By studying the reconstruction in more detail, it is possible to extract quantitative data about the distribution of the particles and the pore filling. Thus examination of the subvolume pore by pore reveals how many particles are present in each mesopore. Figure 3c illustrates this process by showing a single mesopore, extracted from the subvolume, containing two nanoparticles. This process can be repeated for each pore in turn. An animation of a depth analysis can be found online[17] (movie S2). By counting the particles (each of which has a mass of only 2 zeptograms (2×10^{-21} g)) and measuring the internal surface area of the silica from the reconstruction, we determine the *local* catalyst loading, which, for this subvolume, is 1.4×10^{-5} g m^{-2}. To our knowledge, no other technique can provide this local nanoscale information.

It is difficult to state accurately the 3D resolution seen in the tomographic reconstruction of Figures 2 and 3. Certainly the pore structure, with diameter ∼3 nm, is well resolved, as are the individual particles (12-atom clusters), known to be less than 1 nm in diameter. Thus we estimate that, using STEM tomography, coupled with an iterative reconstruction algorithm

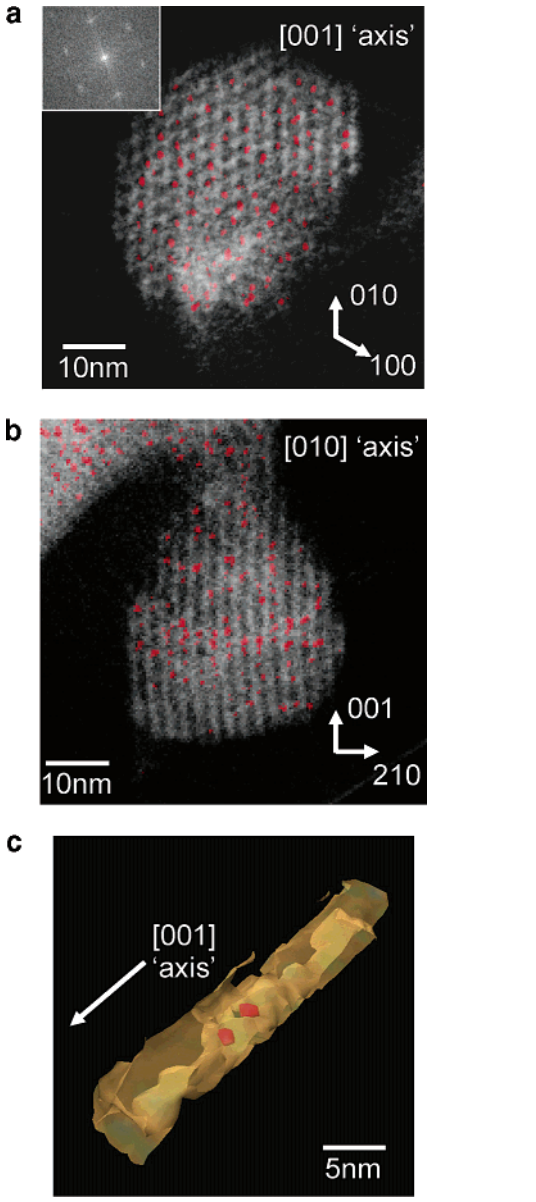

Figure 3. Two perpendicular voxel projections (a) and (b) of the reconstruction volume boxed in Figure 2. In (a) the hexagonal order of the mesoporous silica is evident (inset shows the image power spectrum) and in (b) it is possible to see how the pores are filled with the nanoparticles. (c) is a surface render of a single mesopore extracted from the volume to reveal two nanoparticles within its interior.

described in the Methods, we have demonstrated a tomographic resolution of ∼1 nm in all three dimensions.

In addition to locating precisely their position, by the atomic number contrast seen in STEM HAADF images, it is also possible to determine the elemental composition of the bimetallic particles within the structure using STEM X-ray microanalysis. Figure 4a shows a STEM HAADF image of a catalyst area similar to that shown in Figure 2. The image was acquired with a probe slightly larger (∼0.7 nm) than used for Figure 2 to generate a higher X-ray signal. An X-ray line-spectrum was acquired across three isolated particles indicated in the inset of Figure 4a, and the Pt and Ru counts were plotted in Figure 4b. By measuring the areas of the peaks in Figure 4b and using well-known calibration factors,[18] we determined the ratio of Ru to Pt for all three particles to be 5:1, consistent with the prepared bimetallic composition of $Ru_{10}Pt_2$. The combination

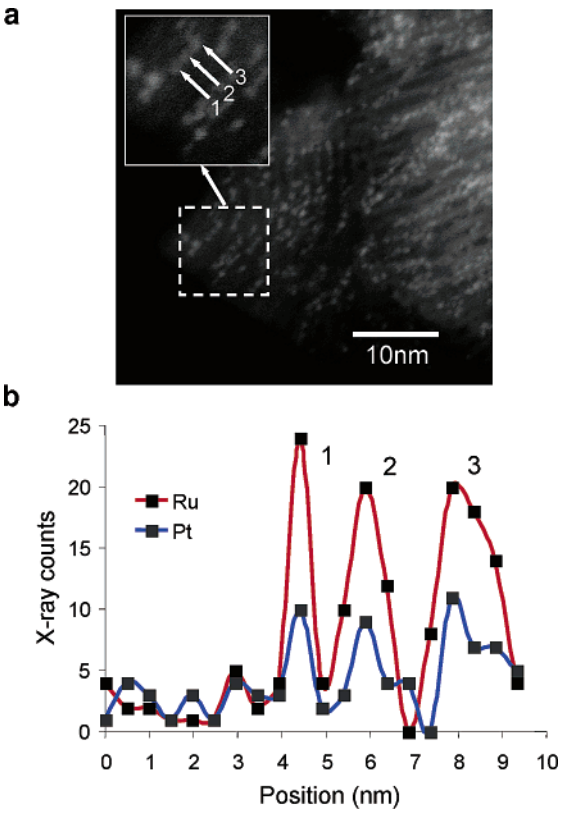

Figure 4. (a) STEM HAADF image of the Ru−Pt-based catalyst. The inset shows the particles studied by X-ray microanalysis. X-ray spectra were recorded approximately every 0.5 nm and the resulting compositional profile across the 3 particles is shown in (b). From the area under the curve in the region of the three nanoparticles, the ratio of Ru:Pt for each particle is determined[18] as 5:1, in line with the composition expected[8] from stripping the carbonyl groups from the precursor ($Ru_{10}Pt_2(CO)_{28}$) dianions.

of STEM tomography and X-ray microanalysis provides both structural and chemical information hitherto unavailable by any technique.

Acknowledgment. We acknowledge financial support from the EPSRC, The Isaac Newton Trust and the Royal Commission for the Exhibition of 1851.

Supporting Information Available: Images of the catalyst reconstructions mentioned in the text from which Figures 2 and 3 are derived and a more detailed description of the catalyst synthesis and the electron microscopy techniques. The material is available free of charge via the Internet at http://pubs.acs.org.

References and Notes

(1) Hart, R. G. *Science* **1968**, *159*, 1464. Crowther, R. A.; de Rosier, D. J.; Klug, A. *Proc. R. Soc. London A* **1970**, *317*, 319. Auer, M. *J. Mol. Med.* **2000**, *78*, 191.

(2) Medalia, O.; Weber, I.; Frangakis, A. S.; Gerisch, G.; Baumeister, W. *Science* **2002**, *298*, 1209.

(3) Marsh, B. J.; Mastronarde, D. N.; Buttle, K. F.; Howell, K. E.; McIntosh, J. R. *Proc. Nat. Acad. Sci. U.S.A.* **2001**, *98*, 2399.

(4) de Jong, K. P.; Koster, A. J. *ChemPhysChem* **2002**, *3*, 776.

(5) Thomas, J. M.; Raja, R.; Sankar, G.; Johnson, B. F. G.; Lewis, D. W. *Chem.: Eur. J.* **2003**, *7*, 2972.

(6) Thomas, J. M.; Johnson, B. F. G.; Raja, R.; Sankar, G.; Midgley, P. A. *Acc. Chem. Res.* **2003**, *36*, 20.

(7) Thomas, J. M.; Raja, R.; Sankar, G.; Bell, R.; Lewis, D. W. *Pure Appl. Chem.* **2001**, *73*, 1087.

(8) Thomas, J. M.; et al. *Chem Commun*. **2003**, *10*, 1126.

(9) Editor's Choice. Renewable Nylons. *Science* **2003**, *300*, 867.

(10) Cortright, R. D.; Davda, R. R.; Dumesic, J. A. *Nature* **2002**, *418*, 964.

(11) Hawkes, P. W. In: *Electron tomography: three-dimensional imaging with the transmission electron microscope*; Frank, J., Ed.; Plenum Press: New York, London, 1992; pp 17−38.

(12) Pennycook, S. J. *Ultramicroscopy* **1989**, *30*, 58.

(13) Howie, A. *J. Microsc.* **1979**, *117*, 11.

(14) Krivanek, O. L.; Nellist, P. D.; Dellby, N.; Murfitt, M. F.; Szilagyi, Z. *Ultramicroscopy* **2003**, *96*, 229.

(15) Midgley, P. A.; Weyland, M.; Thomas, J. M.; Johnson, B. F. G. *Chem. Commun*. **2001**, *18*, 907.

(16) Midgley, P. A.; Weyland, M. *Ultramicroscopy* **2003**, *96*, 413.

(17) Further details regarding the synthesis of the catalyst and the electron microscopy techniques can be found on line at http://pubs.acs.org.

(18) Cliff, G.; Lorimer, G. W. *J. Microsc.* **1975**, *103*, 203.